One-pot Synthesis of N-doped Reduced Graphene Oxide Decorated with Au-Pd@Au Alloy Nanodendrites for Electrochemical Detection of Chrysophanol

Ling Shi[1,2], Ze-Feng Wang[1,2] *, Na Wu[1,2], Gao-Zhang Gou[1,2], Xian-Lan Chen[1,2], Guang-Ming Yang[1,2,*], Wei Liu[1,2,*]

[1] School of science, Honghe University, mengzi, Yunnan 661199, PR China
[2] Key Laboratory of Natural Pharmaceutical & Chemical Biology of Yunnan Province, Mengzi, Yunnan 661199, PR China
*E-mail: wangzefeng841006@163.com , yangguangmingbs@126.com , liuwei4728@126.com

We demonstrate for the first time a new one-step effective route for the preparing of N-doped reduced graphene oxide loading with Au-Pd@Au (N-rGO-Au-Pd@Au) alloy nanodendrites. Then the prepared N-rGO-Au-Pd@Au alloy nanodendrites were used to fabricate a sensitive electrochemical sensor for chrysophanol. The reaction mechanism of chrysophanol on the N-rGO-Au-Pd@Au alloy nanodendrites modified glass carbon electrode was thoroughly investigated by cyclic voltammetry. The impact conditions were optimized by differential pulse voltammetry (DPV). The results showed that the sensor proved high electrocatalytic activity for the determination of chrysophanol. The linear range of chrysophanol is 1.84-84.5 μg mL^{-1} with the detection limit of 0.58 μg mL^{-1}. It is note that the proposed electrochemical sensor was successfully employed to detect real sample. This work may provide an effective analytical platform for determination of chrysophanol in biochemical, pharmaceutical, and clinical research.
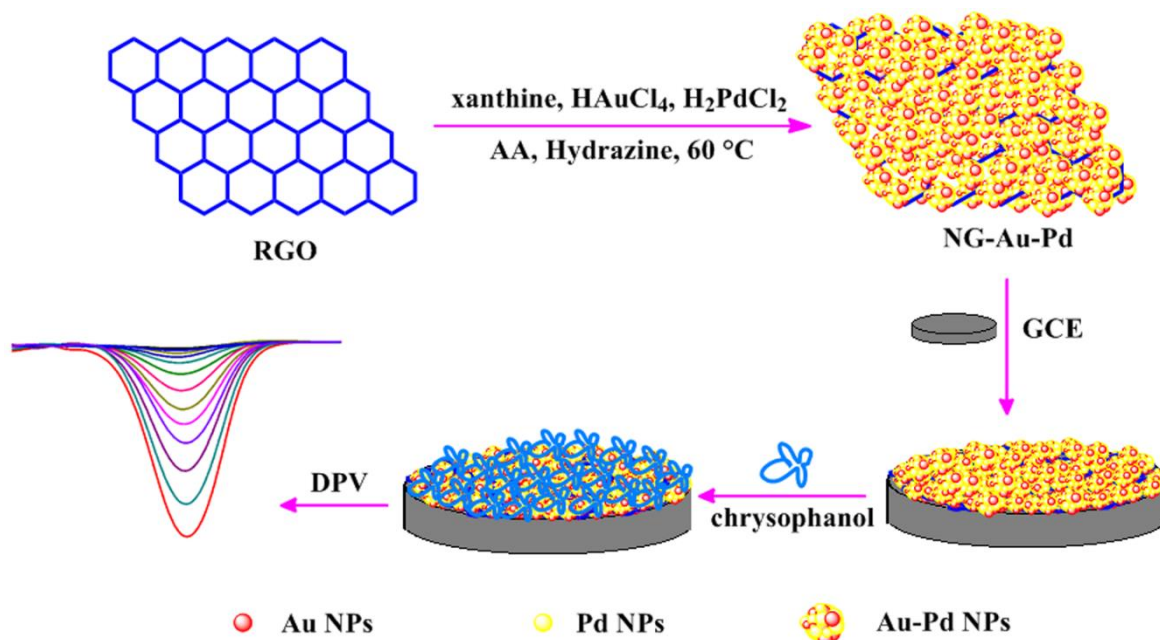
1. INTRODUCTION

Chrysophanol is one of the major anthraquinone and is an active ingredient of medicinal plant rhubarb [1, 2]. Pharmacological research reveals that chrysophanol has strong anti-inflammatory activity, anti-fibrotic, anti-cancer action and anti-microbial activity, which usually used to therapy of gastrointestinal indigestion, obstipation, jaundice and diarrhea in Chinese clinics [3, 4]. Hence, detection of the content of chrysophanol in plant rhubarb is very significant for the quality control of

medicinal herb and its products. Thus, constructing a sensitive, precise, and simple technology for determination of chrysophanol is an important and crucial work in clinical application. Recently, several analytical technology have been developed for determination of chrysophanol, for example, gas chromatography-mass spectrometry [5], high-performance liquid chromatography [6], and capillary electrochromatography [7]. Nevertheless, these analysis technologies usually have complex pretreatment procedures, intricate operate process, long-time detection, and expensive apparatuses. The electrochemical analysis technology has attracted much attention due to instrument simplicity, easyto-operate, low cost, fast response and excellent sensitivity [8, 9].

It is well known that the performance of electrochemical sensors can be effectively improved by introducing nanomaterials due to its high specific surface area, unique electronic structures, and abundant active sites. Hence, synthesized nanomaterials with desired selectivity and electrochemical activity are very crucial. The heterogeneous nanomaterials are considered as promising alternatives in electrocatalytic applications. Recently, alloy nanoparticles have attracted great attention in electrochemical research due to their excellent activity, outstanding chemical stability, superb selectivity, and so on [10]. Au-Pd bimetallic nanoparticles are of increasing interest due to their high miscibility and astonishing activity. For example, Wang and co-workers prepared core/shell structures catalysts of Au-Pd-rGO with excellent catalysts performance [11]. Fang et al reported that Au/Pd bimetallic nanocrystals which have enhanced electrocatalytic performance toward ethanol oxidation [12]. Han prepared Pd-Au bimetallic catalysts which can selective oxidation of acetaldehyde [13]. However, pure alloy nanoparticles are liable to aggregate during the synthetic process and that will affect electrochemical performance. These issues can be efficiently overcome by anchoring the nanoparticles onto specific supports [14, 15]. Recently, nitrogen doped graphene has been widely used in sensor due to the doped graphene with heteroatoms can effectively change elemental composition, which produces considerable number of defects into its lattice on the graphene surface. Furthermore, the introduction of nitrogen element on the graphene can effectively load metal nanoparticles. The combination of nitrogen doped graphene and Pd-Au alloy nanoparticles can obtain a new material possessing unique properties, for example, large surface area, distinctive activity, high conductivity, good stability, excellent selectivity, enhanced catalytic activity, which will greatly broadens the applications of obtained nanomaterials.

In this work, we design a new one-step effective route for synthesizing N-doped reduced graphene oxide decorated with Au-Pd@Au (N-rGO-Au-Pd@Au) alloy nanodendrites. In this synthesis, N-rGO plays an important effect on the nucleation and growth of Au-Pd@Au on its surface. The prepared N-rGO-Au-Pd@Au alloy nanodendrites are used to modify glass carbon electrode, constructing a sensing film for determination of chrysophanol. Scheme 1 shows the strategy for preparing N-rGO-Au-Pd@Au alloy nanodendrites and sensing chrysophanol by an electrochemical strategy. The detection conditions are optimized and the chrysophanol is detected.

Scheme 1. Schematic illustration of the synthesis of the N-rGO-Au-Pd@Au alloy nanodendrites and sense chrysophanol by an electrochemical strategy.

2. EXPERIMENTAL

2.1 Materials

HAuCl$_4$ and K$_2$PdCl$_4$ were obtained from Shanghai sybridge Chemical reagent Company. Xanthine, NaOH, hydrazine, ascorbic acid and chrysophanol were purchased from Shanghai Chemical Reagent Co. Ltd. (Shanghai, China). Graphite (99.95%, 8000 mesh) powders were obtained from Alfa Aesar. Chrysophanol was dissolved into ethanol to prepare 4 mg mL^{-1} standard solution and stored in the fridge at 4 ℃. Ultra-pure water was obtained with a Milli-Q plus water purification system (Millipore Co. Ltd.) (18 M).

2.2. Synthesis of N-rGO-Au-Pd@Au alloy nanodendrites

Graphene oxide (GO) was obtained through modified Hummers' method [16]. The nitrogen-doped reduced graphene oxide supported Au-Pd@Au alloy nanodendrites were prepared by one-step synthesis using GO, HAuCl$_4$, K$_2$PdCl$_4$ and xanthine as raw materials. Briefly, 13.5 mg of as-prepared GO was dispersed in 20 mL of ultra-pure water by ultrasonication for 30 min to obtain a yellow-brown GO solution. 15.21 mg of xanthine was dissolved into 10 mL of ultra-pure water containing 150 μL of NaOH (1 M). Then HAuCl$_4$ (2 mM) and H$_2$PdCl$_4$ (2 mM) and xanthine solution were successively added into above GO solution. The obtained solutions were stirred at 60℃. Then ascorbic acid (10 mM) was added and kept stirring for 40 min. Subsequently, 16.7 M hydrazine solution was dropwise added and the reaction mixtures were stirred at 60℃ for 0.5 h. The obtained solutions were washed with

ethanol and ultrapure water.

2.3. Materials characterization

Transmission electron microscope (TEM) and high-resolution TEM (HRTEM) images were carried out on JEM-2100 TEM (JEOL Ltd.). X-ray Diffraction analysis was performed on X'Pert[3] powder diffractometer (PANAlytical Company). X-ray photoelectron spectra (XPS) studies were carried out on a K-Alpha[+] spectrometer (Thermo fisher Scientific). The electrochemical experiments were performed on CHI660E electrochemical workstation. Nanohybrids-modified glass carbon electrode (GCE, 3mm diameter) served as working electrodes, while Ag/AgCl electrode and Pt wire were used as the reference and counter electrode, respectively. To prepare the working electrode, bare GCE was thoroughly polished with Al_2O_3 (0.3 and 0.05 µm), then sonicated successively in 1:1 nitric acid solution, ethanol and ultrapure water, and then dried in a stream of nitrogen gas. Then 1 mg of as-prepared N-rGO-Au-Pd@Au alloy nanodendrites was dispersed into 1 mL ultrapure water with bath sonication. 7 µL of N-rGO-Au-Pd@Au suspension was dropped onto GCE and dried in air. 0.1 M acetate buffer solutions were used as supporting electrolyte in all cyclic voltammetrys (CVs) and differential pulse voltammetry (DPV) experiments. And a certain amount of chrysophanol was added into the electrochemical cell. An open-circuit accumulation was performed before detection. The DPV was performed with potential increment of 4 mV, amplitude of 50 mV, pulse width of 0.04 s, and pulse period of 0.5 s, respectively.

2.4. Real Sample Assay

The traditional Chinese medicine of rhubarb was obtained from a local pharmacy, and then treated according to the reported method [17]: The rhubarb was pulverized, then 50 mg of the powder was accurately weighed and extracted with 25 mL ethanol for 30 min by ultrasonic extraction. And then the extraction solution was isolated by centrifugation, the supernatant was collected. The obtained solution by diluted to 50.0 mL with ethanol for further analysis.

3. RESULT AND DISCUSSION

3.1. Synthesis and characterization of the N-rGO-Au-Pd@Au alloy nanodendrites

Well dispersed Au-Pd@Au alloy nanodendrites were decorated on N-doped reduced graphene oxide by co-reduction of $HAuCl_4$/K_2PdCl_4 mixtures and GO in the presence of ascorbic acid, hydrazine and xanthine (scheme 1). Figure 1A and B display the typical TEM images of the prepared Au-Pd@Au alloy nanodendrites at different magnifications. The Au-Pd@Au alloy nanoparticles are found to consist of well-dispersed nanodendrites and the overall size is about 25 nm. Figure 1C and D show the TEM images of N-rGO-Au-Pd@Au alloy, Au-Pd@Au alloy nanodendrites are uniformly distributed over the N-rGO nanosheets with an overall size of 25 nm. The N-rGO shows a nearly transparent

flake-like shape. The high-resolution TEM (HRTEM) image show that Au-Pd@Au alloy nanodendrites are multipods with tips about 4.8 nm in diameter (Figure 1E). And the boundaries and voids between the components are present. Figure 1F clearly exhibits that the prepared N-rGO-Au-Pd@Au alloy nanodendrites have a good crystalline structure with well-defined lattice fringes. The lattice planes with an interplanar distance of about 0.23 nm and 0.19 nm, corresponding to the (111) and (200) plane of face-centered cubic (fcc) metallic Au and Pd [18, 19]. The Au-Pd@Au alloy nanodendrites exhibit good crystalline structure.
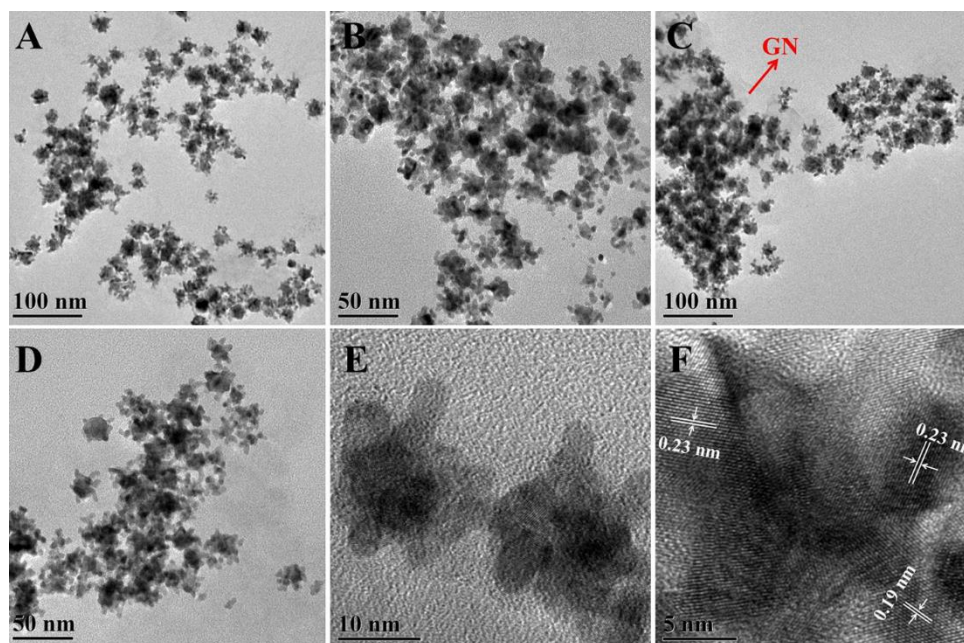

Figure 1. (A) Low- and (B) medium-magnification TEM images of Au-Pd@Au alloy nanodendrites. (C) Low- and (D) medium-magnification TEM images of N-rGO-Au-Pd@Au alloy nanodendrites. (E-F) The HRTEM images of N-rGO-Au-Pd@Au alloy nanodendrites.

In the process of preparing N-rGO-Au-Pd@Au alloy nanodendrites, xanthine plays a crucial role in the formation of crystalline nanodendrites and can be used as nitrogen source and green growth-directing agent [20]. Xanthine can adsorb onto the surfaces of GO *via* π-π interaction. Oxygen-containing groups on the GO were removed in the presence of reductant and the resulting defects on the rGO. That will provide active sites for nitrogen doping. The nitrogen atoms on N-rGO nanosheets can attract $AuCl_4^-$ and $PdCl_4^{2-}$ by electrostatic self-assembly, resulting the uniform distribution of $AuCl_4^-$ and $PdCl_4^{2-}$ on the surface of N-rGO. $AuCl_4^-$ and $PdCl_4^{2-}$ were controlled reduction under the presence of reductant. The control of the reduction rate is crucial to the formation of the Au-Pd@Au alloy nanodendrites. The reduction potential of $AuCl_4^-/Au^0$ (1.002 eV *vs*. SHE) is much higher than that of $PdCl_4^{2-}/Pd^0$ (0.591 eV *vs*. SHE) [21, 22]. Hence, $AuCl_4^-$ was preferentially reduced over Pd^{2+} reduced when Au^{3+} and Pd^{2+} were simultaneously adsorbed on the surface of N-rGO. Otherwise, it is extremely critical that the coexistence of AA and hydrazine were used as reducing agent. Ascorbic acid as a mild reductant, has a slow reduction process of the metal precursor and a low nucleation rate will

result in the formation of bigger Au nanoparticles in the very beginning. Then $AuCl_4^-$ and $PdCl_4^{2-}$ will be co-reduced simultaneously with the initial large particles as the nucleation center when added hydrazine. The precursors can be quickly reduced, nucleation and growth of particles due to the hydrazine has a strong reducing capacity. The combined action of hydrazine and ascorbic acid will result formation of Au-Pd@Au alloy nanodendrites *via* nucleation, epitaxial crystal growth. Moreover, ascorbic acid might promote the formation of multipodal or porous particles [23].

In order to further investigate the crystalline structure of prepared N-rGO-Au-Pd@Au alloy nanodendrites, the nanohybrids were characterized with X-ray diffraction (XRD) pattern (Figure 2). A broad diffraction is observed at about 26.1°, which is corresponding to the 002 planes of the N-rGO [8]. The typical diffraction peaks located at 2θ=38.19°, 44.85°, 65.10°, and 77.54°, which are coincidently located at Au NPs (reference code: 00-004-0784) can be indexed as the (111), (200), (220), and (311) reflections of the fcc Au NPs. The diffraction peaks at about 39.35°, 45.79°, 67.13°, and 80.86°, which are coincidently located at Pd NPs (reference code: 00-005-0681) can be indexed as the (111), (200), (220), and (311) reflections of the fcc Pd NPs [24, 25]. Notably, each diffraction peak has synergistic influence result the diffraction peak to broaden. The results further suggest that the prepared N-rGO-Au-Pd@Au alloy nanodendrites are alloy structure.
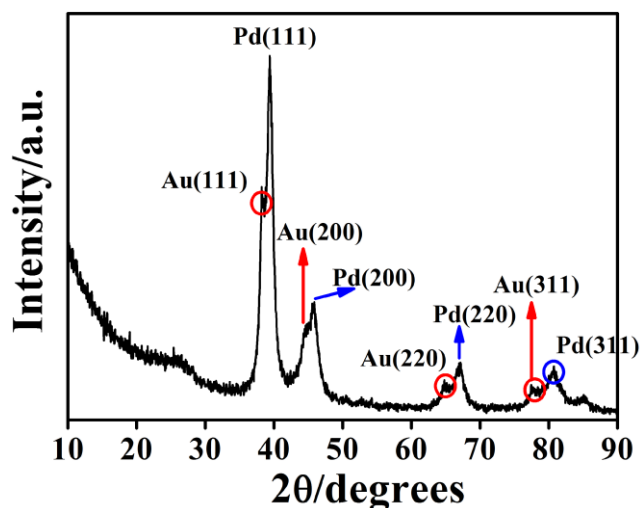

Figure 2. XRD patterns of N-rGO-Au-Pd@Au alloy nanodendrites.

N-rGO-Au-Pd@Au alloy nanodendrites were detected by X-ray photoelectron spectroscopy (XPS). As shown in Figure 3A, the dominant XPS peaks at 84.36, 293.06, 349.86, 400.01, and 540.86 eV come from Au 4f, C 1s, Pd 3d, N 1s, and O 1s in the survey spectrum, respectively, which reveals the existence of C, O, N, Au and Pd elements in the N-rGO-Au-Pd@Au nanodendrites. Figure 3B shows the peak fitting of high-resolution C 1s region. The peaks at 284.7, 286.1, and 288.4 eV, corresponding to the C-C, C-O/C-N, O-C=O, respectively [26, 27]. The sp^2-hybridized graphene C-C peaks are assigned to the graphitic structure. It is noteworthy the presence of the C-N bond at 286.1 eV which further confirming the successfully doping of N into rGO. The N1s high resolution spectrum shows two different electronic states (Figure 3C), the binding energies centered at 399.6 eV and 400.0

eV, which correspond to the -NH- and -N$^+$- [28, 29]. For the high resolution O 1s spectrum can be deconvoluted into two peaks: C=O at 531.5 eV and C-O at 533.0 eV is presented in Figure 3D [30]. Figure 3E displays the high-resolution XPS spectrum of Au 4f. One pair at 83.71 eV and 87.40 eV representing Au 4f$_{7/2}$ and Au 4f$_{5/2}$ of metallic Au^0 species, the other two peaks at 84.14 and 88.07 eV are attributed to the cationic Au^{3+} species [20, 31]. It should be noted that a small fraction of Au^{3+} exists in N-rGO-Au-Pd@Au alloy nanodendrites, which is possibly attributed to the strong physical absorption between cationic Au^{3+} species N-rGO [32, 33]. The Pd 3d region can be fitted four peaks (Figure 3F), the two peaks located at 335.20 and 340.40 eV attributed to the metallic Pd. While the other two peaks emerged at 338.44 eV and 343.85 eV correlated to Pd^{2+} species [34, 35]. While the other two small peaks appear at are assigned to the cationic Pd^{2+}species.
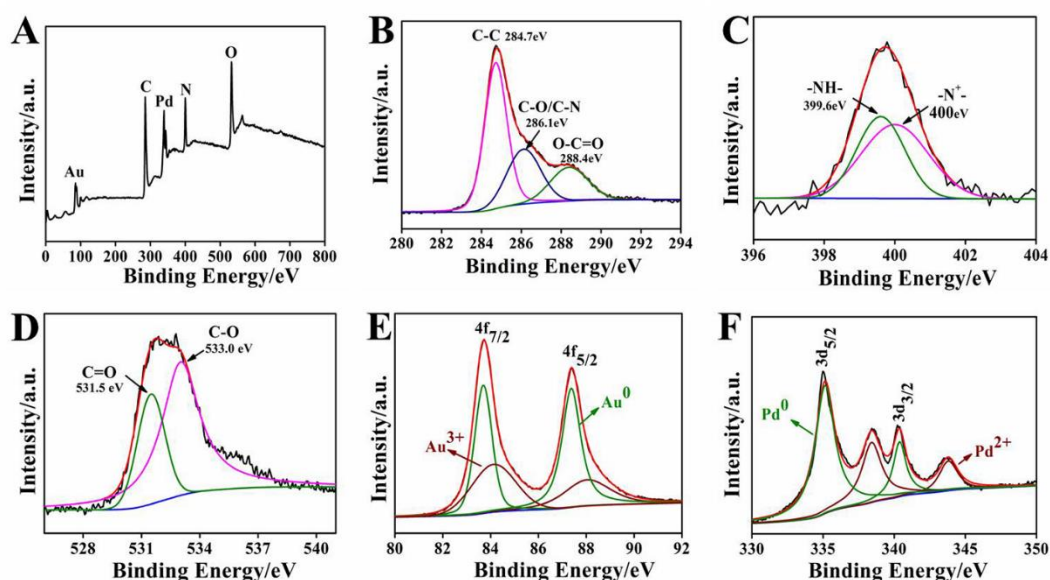

Figure 3. (A) XPS survey spectra of N-rGO-Au-Pd@Au alloy nanodendrites; high resolution (B) C1s, (C) N1s, (D) O1s, (E) Au 4f and (F) Pd 3d spectra of N-rGO-Au-Pd@Au alloy nanodendrites.

3.2. Effect of pH

The pH represents a significant impact on the electrochemical response of chrysophanol at N-rGO-Au-Pd@Au/GCE. The influence of pH was investigated by measuring the differential pulse voltammograms in 0.1 M acetate buffer solutions containing 50.14 μg mL^{-1} chrysophanol over the pH range from 3.0 to 5.6. The results are illustrated in Figure 4. It is observed that the oxidation peak potential of chrysophanol is shifted towards the negative potential direction with increasing pH of supporting electrolyte which suggests proton-coupled electron transfer [36]. In addition, the oxidation peak current values changed as the varied of solution pH, and a maximum peak current obtained at pH 3.6. Therefore, acetate buffer of pH=3.6 is employed for the subsequent experiments.
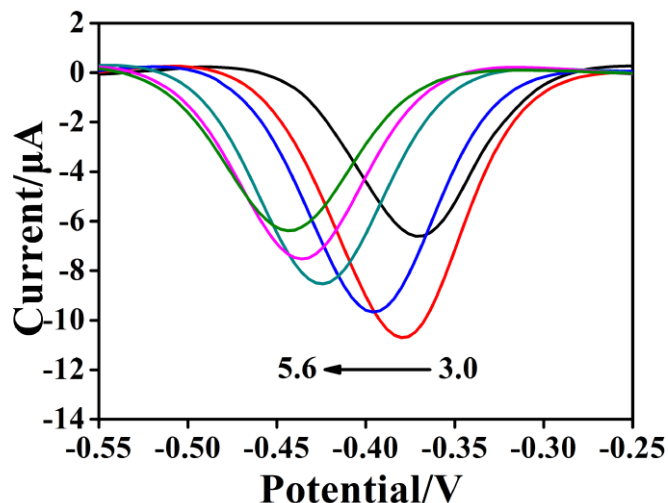
Figure 4. DPV curves of 50.14 μg mL^{-1} chrysophanol on N-rGO-Au-Pd@Au/GCE in 0.1 M acetate buffer solutions with different pH values. Accumulation was performed under open-circuit for 3 min.

3.3. Effect of scan rate

Electrochemical reaction mechanism of chrysophanol at N-rGO-Au-Pd@Au/GCE was investigated by CV. Figure 5a displays the CVs of N-rGO-Au-Pd@Au/GCE in pH=3.6 acetate buffer solutions containing 50.14 μg mL^{-1} of chrysophanol at different scan rates (100-1000 mV s^{-1}). It is found that the oxidation peak potential of chrysophanol shifted positively and the reduction peak potential of chrysophanol shifted negatively.
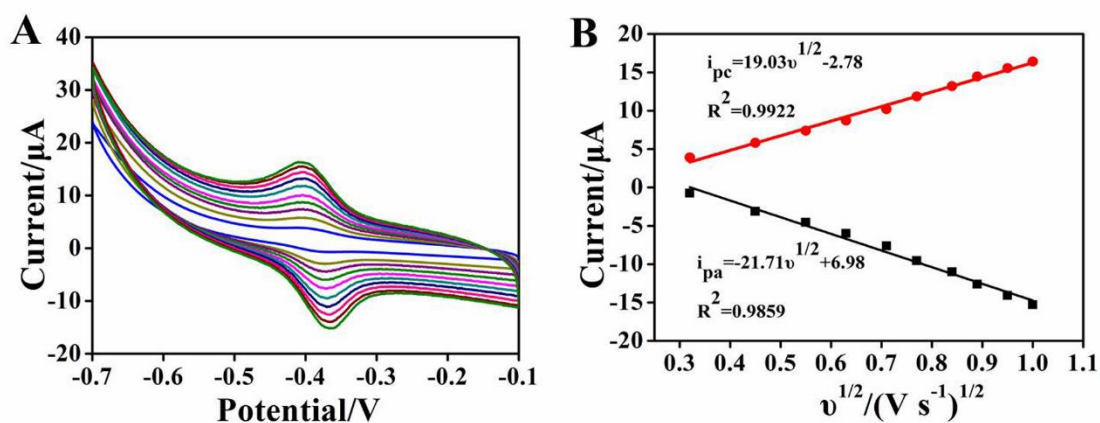

Figure 5. (A) CVs of N-rGO-Au-Pd@Au/GCE in pH = 3.6 acetate buffer solutions containing 50.14 μg mL^{-1} of chrysophanol at scan rate of 100, 200, 300, 400, 500, 600, 700, 800, 900, and 1000 mV s^{-1} (from inner to outer curve). Accumulation was performed under open-circuit for 3 min. (B) Calibration plots of cathodic and anodic peak current versus various scan rates from 100-1000 mV s^{-1}.

The redox peak current increased gradually with increasing of scan rate. Furthermore, the peak

current is linearly increased with square root of the scan rate ($\nu^{1/2}$), and the regression equation is described as $I_{pa}(\mu A)=-21.71\nu^{1/2}(V/s)^{1/2}+6.98$ with a correlation coefficient of $R^2=0.9859$; $I_{pc}(\mu A)=19.03\nu^{1/2}(V/s)^{1/2}-2.78$ with a correlation coefficient of $R^2=0.9922$ (Figure 5b). This reveals that the electrocatalytic oxidation of chrysophanol at N-rGO-Au-Pd@Au/GCE is a typical diffusion-controlled process [37].

3.4. Effect of suspension volume and accumulation time

The amount of nanocatalyst is an important factor for the detection of chrysophanol. The relationship between the oxidation peak current of chrysophanol and suspension volume from 1 to 11 µL of N-rGO-Au-Pd@Au was investigated by DPV. The results as shown in Figure 6A, the oxidation peak currents increased remarkably with the increasing suspension volume from 1 to 7 µL. That can be due to the increasing number of modifiers on the bare GCE surface and further improved ability to capture chrysophanol. The peak current then remained unchanged, revealing overmuch suspension will lead to thicker film, which can obstruct the interface electron transfer. Thus, the optimal volume of 7 µL is employed in our experiments.
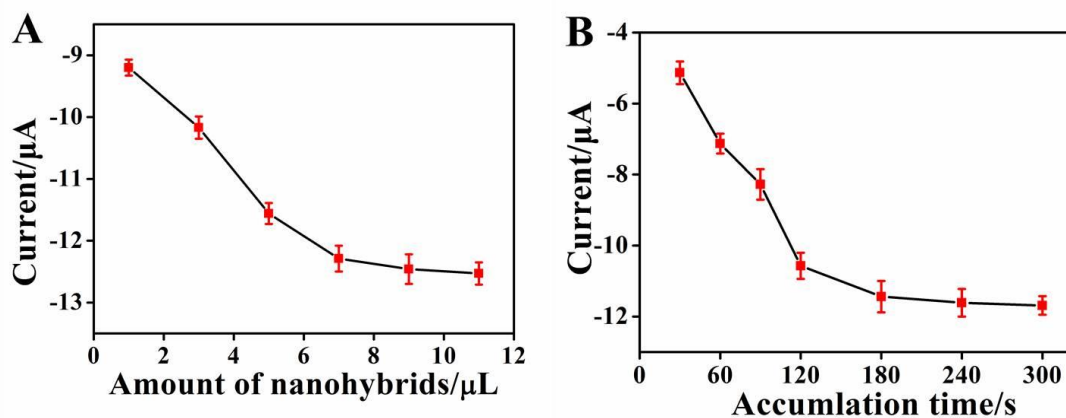

Figure 6. (A) Influence of the amount of N-rGO-Au-Pd@Au alloy nanodendrites on oxidation peak current of 50.14 µg mL^{-1} chrysophanol. (B) Influence of accumulation time on the oxidation peak current of 50.14 µg mL^{-1} chrysophanol. Accumulation was performed under open-circuit for 180 s. Error bar represents the standard deviation of triple measurements.

When considering the electrochemical reaction of chrysophanol on N-rGO-Au-Pd@Au modified GCE, the accumulation time is a critical influencing factor toward the determination of chrysophanol. The effect of accumulation time for the determination of chrysophanol was investigated by DPVs in Figure 6B. The oxidation peak currents increased gradually with the accumulation time increased from 30 s to 180 s indicates a great many of the chrysophanol is adsorbed at the surface of GCE and thereafter the peak current tends to be almost unchanged proving that the adsorption equilibrium is reached. Therefore, 180 s is chosen for chrysophanol accumlation.

3.5. Determination of chrysophanol

The DPV technique was applied to detect chrysophanol at the N-rGO-Au-Pd@Au alloy nanodendrites modified GCE under optimal conditions. Figure 7A depicts the DPV response for different concentration of chrysophanol in acetate buffer solutions. The peak current response increased linearly with the increasing of chrysophanol concentration. As shown in Figure 7B, the calibration curve exhibits a great linear range of 1.84-84.5 µg mL^{-1}. The regression equation is Ipa=-0.573c+0.525 (R^2=0.9987). The detection limit of chrysophanol is calculated to be 0.58 µg mL^{-1} (S/N=3). Obviously, the proposed sensor possesses excellent electrochemical performance maybe due to the unique structure and eminent catalytic activity of the N-rGO-Au-Pd@Au.
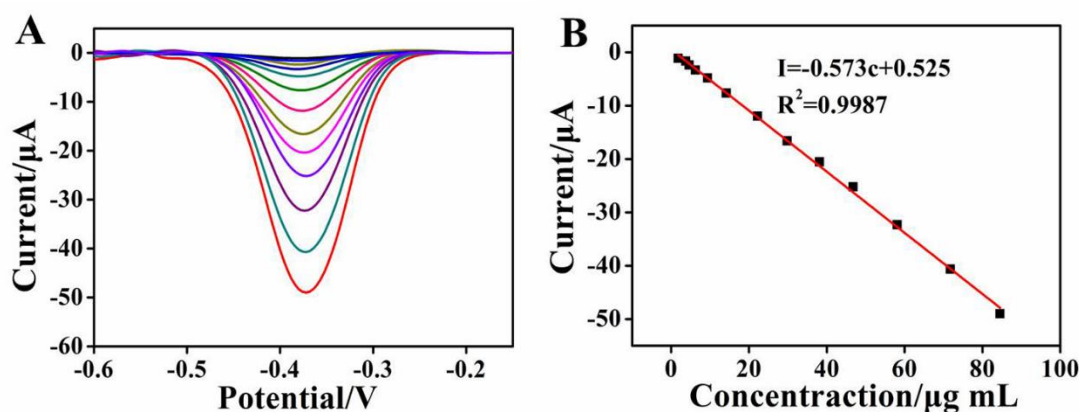

Figure 7. (A) DPV response of the N-rGO-Au-Pd@Au/GCE under optimum conditions for different chrysophanol concentrations: 1.84, 3.76, 4.67, 6.25, 9.39, 14.18, 22.24, 29.85, 38.12, 46.76, 58.13, 71.75, 84.5 µg mL^{-1}. (B) The calibration curves of chrysophanol.

3.6. Real sample analysis

In order to test the feasibility of the proposed sensor for potential application, the sensor was used to detect chrysophanol in rhubarb by using standard addition method. The results are listed in Table 1. The content of chrysophanol in rhubarb is calculated to be about 5.18 mg g^{-1}. The result is in consistent with the other detection method reported in literature [6, 38]. The satisfactory recoveries are obtained from 98.4-103.2%, which indicate that fabricated electrochemical sensor is suitable for practical application. The results indicating that the proposed method is suitable for electrochemical investigation of chrysophanol in biochemical, pharmaceutical, and clinical research.

Table 1. The recoveries of chrysophanol from rhubarb samples (n=3).

	Original found/µg mL	Standard added/µg mL	Total founded/µg mL	Recovery/%
1	5.21	1.25	6.44	98.4
2	5.15	2.50	7.68	101.2
3	5.17	3.75	9.04	103.2

4. CONCLUSION

In this research, we design a new strategy for synthesizing N-rGO-Au-Pd@Au alloy nanodendrites. And then design a novel sensing platform for the electrochemical detection of chrysophanol. The unique structure and excellent electrochemical performance of prepared N-rGO-Au-Pd@Au alloy nanodendrites are benefit to detect chrysophanol. The results show that the sensor possesses wide linear range and good detection limit. Furthermore, the proposed electrochemical sensor can successfully detect chrysophanol in real sample. All of these results prove that this work provide an effective analytical platform for determination of chrysophanol in biochemical, pharmaceutical, and clinical research.

References

1. H. F. Zhang and Y. P. Shi, *Talanta*, 82 (2010) 1010.
2. J. Koyama, I. Morita and N. Kobayashi, *J. Chromatogr. A*, 1145 (2007) 183.
3. L. P. Ma, L. Zhao, H. H. Hu, Y. H. Qin, Y. C. Bian, H. D. Jiang, H. Zhou, L. u. S. Yu and S. Zeng, *J. Ethnopharmacol.,* 153 (2014) 864.
4. K. Chen, C. Q. Wang, Y. Q. Fan, Y. S. Xie, Z. F. Yin, Z. J. Xu, H. L. Zhang, J. T. Cao and Y. Wang, *Int. J. Clin. Exp. Med.,* 8 (2015) 10558.
5. Q. H. Chen, H. S. He, S. W. Luo, L. Xiong and P. Li, *J. Chromatogr. B*, 973 (2014) 76.
6. S. X. Feng, M. M. Li, D. Zhao, X. H. Li, L. Zhang, Z. Wang and N. N. Gao, *Chin. Herb. Med.*, 9 (2017) 388.
7. H. X. Lü, J. B. Wang, X. C. Wang, X. C. Lin, X. P. Wu and Z. H. Xie, *J. Pharm. Biomed. Anal.*, 43 (2007) 352.
8. Z. F. Wang, G. Z. Gou, L. Shi, J. Yang, C. Xu, L. Zhang, A. P. Fan and Y. Min, *J. Appl. Polym. Sci.*, (2018) 4670.
9. E. M. Mximnano, F. D. Lima, C. A. L. Cardoso and G. J. Arruda, *Electrochim. Acta,* 259 (2018) 66.
10. L. Zhang, Z. X. Xie and J. L. Gong, *Chem. Soc. Rev,* 45 (2016) 3916.
11. B. Wang, T. Y. Chang, X. Gong, Z. Jiang, S. Yang, Y. S. Chen and T. Fang, *ACS Sustainable Chem. Eng*, 7 (2019) 1760.
12. C. H. Fang, T. Bi, Q. Ding, Z. Q. Cui, N. Yu, X. X. Xu and B. Y. Geng, *ACS Appl. Mater. Interfaces,* 11 (2019) 20117.
13. S. M. Han, K. Shin, G. Henkelman and C. B. Mullins, *ACS Catal.*, 9 (2019) 4360.
14. X. Chen, G. Wu, J. Chen, X. Chen, Z. Xie and X. Wang, *J. Am. Chem. Soc.*, 133 (2011) 3693.
15. Z. L. Wang, J. M. Yan, Y. F. Zhang, Y. Ping, H. L. Wang and Q. Jiang, *Nanoscale*, 6 (2014) 3073.
16. W. S. Hummers and R. E. Offeman, *J. Am. Chem. Soc.*, 80 (1958) 1339.
17. Y. Y. Zhang, Y. Y. Wang, K. B. Wu, S. C. Zhang, Y. Zhang and C. D. Wan, *Colloids Surf. B.*

Biointerfaces, 103 (2013) 94.

18. S. S. Li, A. J. Wang, Y. Y. Hu, K. M. Fang, J. R. Chen and J. J. Feng, *J. Mater. Chem. A*, 2 (2014) 18177.
19. L. F. Zhang, S. L. Zhong and A. W. Xu, *Angew. Chem., Int. Ed.*, 52 (2013) 645.
20. R. Wang, W. D. Liu, A. J. Wang, Y. D. Xue, L. Wu and J. J. Feng, *Biosensors Bioelectron.*, 99 (2018) 458.
21. L. Kuai, X. Yu, S. Z. Wang, Y. Sang and B. Y. Geng, *Langmuir*, 28 (2012) 7168.
22. L. F. Tan, X. L. Wu, D. Chen, H. Y. Liu, X. W. Meng and F. Q. Tang, *J. Mater. Chem. A,* 1 (2013) 10382.
23. C. H. Kuo and M. H. Huang, *Langmuir*, 21 (2005) 2012.
24. L. H. Shi, A. Q. Wang, T. Zhang, B. S. Zhang, D. S. Su, H. Q. Li and Y. J. Song, *J. Phys. Chem.* C 117 (2013) 12526.
25. Y. W. Lee, M. Kim, Y. Kim, S. W. Kang, J. H. Lee and S. W. Han, *J. Phys. Chem. C*, 114 (2010) 7689.
26. J. Luo, N. Zhang, R. Liu and X. Y. Liu, *RSC Adv.*, 4 (2014) 64816.
27. S. Y. Wang, X. Wang and S. P. Jiang, *Phys. Chem. Chem. Phys.*, 13 (2011) 6883.
28. X. M. Feng, R. M. Li, Y. W. Ma, R. F. Chen, N. E. Shi, Q. L. Fan and W. Huang, *Adv. Funct. Mater.*, 21 (2011) 2989.
29. Q. Wu, Y. X. Xu, Z. Y. Yao, A. R. Liu and G. Q. Shi, *ACS Nano*, 4 (2010) 1963.
30. M. Kotal, A. K. Thakur and A. K. Bhowmick, *ACS Appl. Mater. Interfaces,* 5 (2013) 8374.
31. Z. K. Zheng, B. B. Huang, X. Y. Qin, X. Y. Zhang, Y. Dai and M. H. Whangbo, *J. Mater. Chem.*, 21 (2011) 9079.
32. H. H. Kung, M. C. Kung and C. K. Costello, *J. Catal.,* 216 (2003) 425.
33. A. Y. Klyushin, M. T. Greiner, X. Huang, T. Lunkenbein, X. Li, O. Timpe, M. Friedrich, M. Hävecker, A. KnopGericke and R. Schlögl, *ACS Catal.*, 6 (2016) 3372.
34. H. J. Dong, R. F. Xie, L. Yang and F. Li, *Dalton Trans.*, 47 (2018) 7776.
35. G. Darabdhara, M. R. Das, V. Turcheniuk, K. Turcheniuk, V. Zaitsev, R. Boukherroub and S. Szunerits, *J. Mater. Chem.* B, 3 (2015) 8366.
36. T. E. Chiwunze, V. N. Palakollu, A. A. S. Gill, F. Kayamba, N. B. Thapliyal and R. Karpoormath, *Mater. Sci. Eng.*, C, 97 (2019) 285.
37. A. Zabihollahpoor, M. Rahimnejad, G. Najafpour and A. A. Moghadamnia, *J. Electroanal.* C., 835 (2019) 281.
38. Z. B. Wang, J. X. Hu, H. X. Du, S. He, Q. Li and H. Q. Zhang, *J. Pharm. Biomed. Anal.*, 125 (2016) 178.